Volume 19, Number 3, 2026. pp. 281-302

Jordan Journal of Physics

ARTICLE

New Parameters for Nuclear Forces and Densities Using a New Binding Energy Formula Based on the Earth Model

Alaa Khodari, Abdullah Rastanawi and **Soleiman Dibo**

Department of Physics, Homs University, Homs, Syria.

DOI: **https://doi.org/10.47011/19.3.1**

Received on: 07/12/2024; *Accepted on: 23/07/2025*

Abstract: In this research, a novel formula for the binding energy of all nuclides on the Segre chart was derived based on the solution of the Bateman equation. Building on nuclear reactions and decays, an Earth model was proposed. Utilizing this model, we obtained a binding energy formula that exhibits better agreement with empirical binding energies than the Weizsäcker formula based on the liquid drop model. We determined the coefficients of the binding energy formula related to volume, surface, and Coulomb effects within the three layers of the nucleus and their influence on the nucleus's non-spherical deformation. Modifications were made to the nuclear radius relationship, and a formula for varying nuclear density was established. Furthermore, a differential equation describing the change in binding energy with respect to mass number variation was derived. This equation can serve as a new foundation for understanding nuclear forces and determining the coefficients of nuclear forces between nucleons residing in the three layers of the nucleus.

Keywords: Binding energy, Nuclear forces, Bateman equation, Earth model, Nuclear radius, Nuclear density.

1. Introduction

The absence of a comprehensive understanding of the nucleus has led to the development of several nuclear models (such as the liquid drop model, the Fermi gas model, the shell model). Each model successfully explains certain nuclear properties but fails to account for others. The liquid drop model, for instance, has been successful in formulating nuclear binding energy quite well. A weakness of this formula is that it fails to explain the nature of nuclear forces governing these nuclei or to provide a clear understanding of those forces or their parameters.

In nuclear physics, the semi-empirical mass formula (SEMF), also known as Weizsäcker's formula or the Bethe–Weizsäcker formula [1–3], is used to estimate the masses of nuclei and their binding energies. The theoretical part of this formula was derived from the assumptions of the liquid drop model proposed by George Gamow [4]. The theoretical part includes several terms later introduced by Niels Bohr and John Archibald Wheeler [5]. The formula reached its final form when it was completed by the German physicist Carl Friedrich von Weizsäcker in 1935 [6–7], and it has been in use ever since. According to the above model, the theoretical component of the binding energy of the nucleus consists of the following terms: the volume energy term, the surface energy term, the Coulomb energy term, the asymmetry energy term, and the pairing energy term, as shown in the following equation:

$$E_{Bth}(Z,A) = a_V A - a_S A^{\frac{2}{3}} - a_C \frac{Z(Z-1)}{A^{\frac{1}{3}}} - a_A \frac{(A-2Z)^2}{A} \pm a_P A^{-\frac{1}{2}} \quad (1)$$

In recent years, new nuclear mass models have been proposed [8, 9] to better explain magic numbers. Among these models is the Duflo-Zuker model [10]. In 2002, Samanta et al. [11] expanded the liquid drop model's binding energy formula to include light nuclei. By 2008, Royer et al. [12] revised the mass formula based

Corresponding Author: Alaa Khodari **Email**: a-khodari@homs-univ.edu.sy

on the liquid drop model and added new parameters, such as shape energy, surface correction energy, charge-exchange energy, and Wigner energy. By 2011, Chirashree et al. [13] proposed a new phenomenological formula for nuclear ground-state binding energies. In 2012, Ghahramany et al. [14] made a new approximation to the binding energy formula based on the integrated nuclear model. In this model, the constituent nuclear particles are considered 'free' in a dense plasma-type medium. In 2014, Wang et al. [15] studied the effect of analog surface diffusion, which plays a critical role in the development of neutron shells in heavy nuclei approaching the neutron drip line. The modified Bethe-Weizsäcker relation for spherical nuclei is given by a new global mass formula. Then, in 2020, Hezekiah et al. [16] proposed a modified integrated nuclear model MINM), a simple model based on the numbers of protons and neutrons and a variable stability coefficient factor denoted by λ. In 2022, Aldawdy et al. [17] modified the energy-term parameters in the binding energy formula based on the liquid drop model by adding a new term for closed-shell corrections. In 2024, Pablo [18] developed a new approach to the study of experimental binding energy, the Continued Fraction Regression (cf-r), to analyze the nuclear binding energy B (A, Z). In our previous research [19], we modified the binding energy formula according to the liquid drop model by adding the thermal term, where we considered that every nucleus at room temperature has gained energy in the form of heat, and therefore we focused on the thermal energy gained by stable nuclei as a function of their mass number.

In this research, we focused on a large number of nuclei that are systematically related to each other. This occurs when they are bombarded with particles or when nuclei decay to produce other nuclei. Consequently, nuclear reactions or decay processes involve changes in mass number, which in turn alter the binding energy of the nucleus. Based on the Earth model, we aim to derive a formula for the binding energy based on sequential radioactive-decay equations. We expect that this formula could outperform the binding energy formula derived from the liquid drop model and achieve a better fit to experimental data. It could also help formulate an equation that governs and explains nuclear forces, as well as study nuclear properties such as nuclear radius and density.

2. Theoretical Study

2.1. How to Choose the Studied Nuclide Group?

A total of 3559 nuclides were studied, using data from the AME 2020 atomic mass [20], which contains all experimental data on the atomic masses of measured nuclides as well as the experimental values of nucleon binding energies. These values can also be computed using the Mathcad software based on the following equations:

$$E_{\mathrm{Bexp}}(Z,A) = \left[Z \cdot m_p + N m_n - M\left({}^{A}_{Z}\mathrm{X}\right)\right]c^2 \ \mathrm{MeV} \quad (2)$$

$$E_{\mathrm{Nexp}} = \frac{E_{\mathrm{Bexp}}(Z,A)}{A} \quad (3)$$

Each nuclide has at least one isotope, and up to 18 isotopes. Each nuclide also has a certain number of isobars. The selection of the nuclide set is performed as follows: for a nuclide with a given mass number (e.g., A = 2), the first isobar with the highest experimental binding energy is placed in the first group, the second isobar with the next highest binding energy is placed in the second group, and so on. For another nuclide with a mass number A+1, the isobar with the highest experimental binding energy is placed in the first group, and the second isobar, with the next highest binding energy, is placed in the second group, the third isobar, with a lower energy than the second, is placed in the third group, and so on, and the process continues in this manner to the last nuclide (A = 298). This classification was conducted using the VLOOKUP function in Excel, resulting in 18 groups.

Figure 1 shows a graph of the 18 selected nuclide groups. Figs. 2, 3, and 4 illustrate the average binding energy per nucleon as a function of the mass number of nuclides studied in the first, tenth and thirteenth groups, respectively.

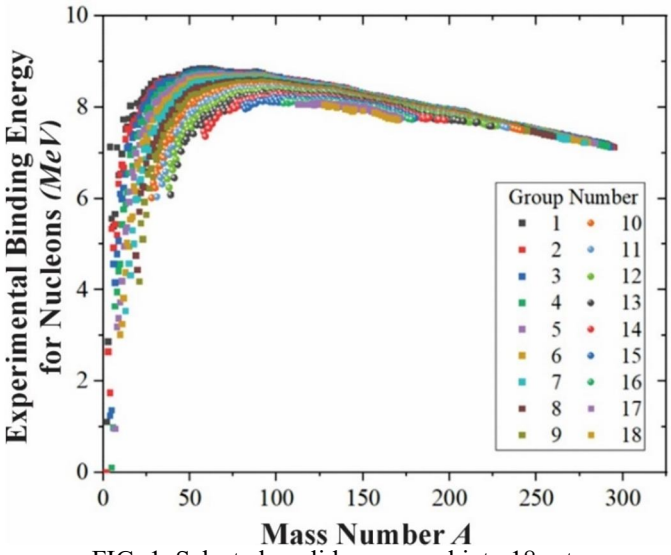

FIG. 1. Selected nuclides grouped into 18 sets.

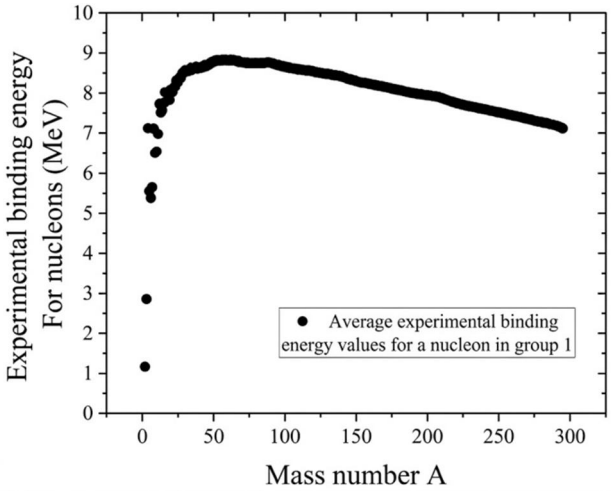

FIG. 2. Experimental binding energy per nucleon for the nuclei of the first group as a function of mass number.

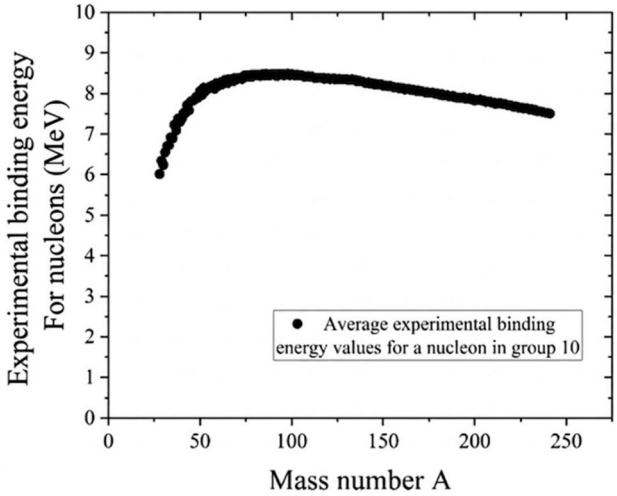

FIG. 3. Experimental binding energy per nucleon for the nuclei of the tenth group as a function of mass number.

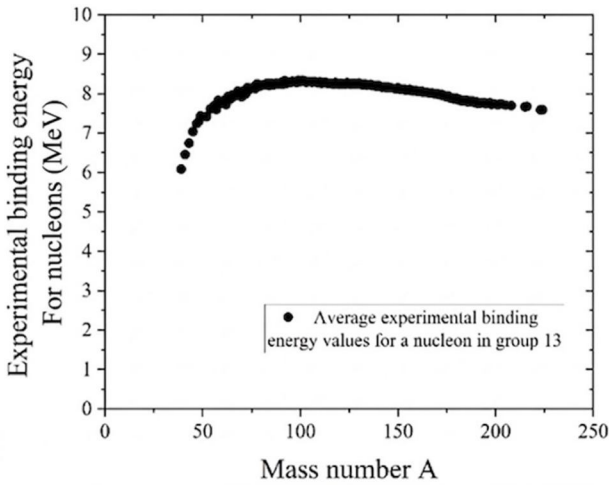

FIG. 4. Experimental binding energy per nucleon for the nuclei of the thirteenth group as a function of mass number.

In this approach, the studied nuclei of each group are arranged as a hypothetical decay chain, in which a nuclide with a lower mass number is considered to be produced from the immediately preceding nuclide with a higher mass number. For example, during a decay process, a nucleus denoted as ${}^{\mathrm{A}}_{\mathrm{Z}}\mathrm{Y}$ transforms into another nucleus, ${}^{A-A_1}_{\mathrm{Z}-Z_1}\mathrm{X}$ which has a different binding energy. However, the binding energy of the resulting nucleus remains close to that of the parent nucleus ${}^{\mathrm{A}}_{\mathrm{Z}}\mathrm{Y}$.

$$ {}^{\mathrm{A}}_{\mathrm{Z}}\mathrm{Y} \longrightarrow {}^{A-A_1}_{\mathrm{Z}-Z_1}\mathrm{X} + {}^{A_1}_{Z_1}y \tag{4} $$

In a nuclear reaction triggered by the bombardment of ${}^{\mathrm{A}_2}_{\mathrm{Z}_2}\mathrm{Z}$ with an unknown virtual particle ${}^{A_1}_{Z_1}y$, the resulting products are expressed by:

$$ {}^{A_2}_{Z_2}\mathrm{Z} + {}^{A_1}_{Z_1}y \rightarrow {}^{\mathrm{A}-\mathrm{A}_2}_{\mathrm{Z}-\mathrm{Z}_2}\mathrm{Y} + {}^{\mathrm{A}_2}_{\mathrm{Z}_2}\mathrm{y} \tag{5} $$

where ${}^{A_1}_{Z_1}y, {}^{\mathrm{A}_2}_{\mathrm{Z}_2}\mathrm{y}$ represents the nuclide or a produced virtual particle from the nuclear decay or reaction.

Each group is studied as if it were a nuclear reaction or decay series similar to natural radioactive decay chains. Thus, nuclei result from the sequential decay of other nuclei, where the number of nuclei N changes over time t in a series, as depicted in the following formula:

$$ N_1(t) \rightarrow N_2(t) \rightarrow N_3(t) \rightarrow \cdots \rightarrow N_n(t) $$

The radioactive decay chains obey the general sequential (series) radioactive decay equation, derived by solving the Bateman equation [21, 22]:

$$ N_n(t) = N_1^0\left(c_1 e^{-\lambda_1 t} + c_2 e^{-\lambda_2 t} + \cdots + c_n e^{-\lambda_n t}\right) \tag{6} $$

Consequently, since the number of nuclei changes during decay or nuclear reactions, the change in nucleon number leads to a change in the experimental binding energy of the resulting nuclei as a function of mass number, forming a series, as shown in the following formula:

$$ E_1(A) \rightarrow E_2(A) \rightarrow E_3(A) \rightarrow \cdots \rightarrow E_n(A) $$

Thus, the form of the newly proposed nuclear binding energy formula for the studied isotope groups $E_n(A)$ mirrors the form of $N_n(t)$ for all the studied nuclear groups depicted in Fig. 1.

$$ E_n(A) = a_0 e^{-a_1 A} + a_2 e^{-a_3 A} + a_4 e^{-a_5 A} + \cdots + a_n e^{-a_{n+1} A} \tag{7} $$

Since the experimental binding energy is determined by Eqs. (2) and (3) based on mass measurements using mass spectrometry at a specific temperature, and since nuclear reactions and decays are accompanied by changes in internal thermal excitation energy, the nucleus cannot be strictly approximated as a liquid drop—as assumed in the liquid drop model—neither at absolute zero temperature nor at elevated temperatures. At absolute zero, nucleons fill the lowest energy levels in the nuclear potential well (below the Fermi level), exhibit high density and are controlled by the nuclear forces, as in a solid. As the internal thermal excitation energy associated with nuclear processes increases, nucleons gain kinetic energy and jump above the Fermi level. Consequently, the nucleus behaves

metaphorically as a liquid-like state of intermediate density, where nuclear and Coulomb forces balance; finally, a gas-like state of low density is formed, and long-range Coulomb forces dominate. This progression aligns with the empirical Woods-Saxon density distribution and the Woods-Saxon potential formula. Building on this, we propose an Earth-model-inspired conceptualization of the nucleus as an object with three distinct density layers: an inner core (solid phase) of highest density, an intermediate layer (liquid phase**)** of lower density, and a surface layer (gaseous phase) of lowest density. Each term in the theoretical binding energy formula can thus be related to one of these three nuclear layers. Therefore, under specific conditions and in particular cases, this model integrates three theoretical frameworks, the shell model, the liquid drop model, and the Fermi gas model, while remaining based on empirical values. We then tested the fit of the proposed nuclear binding energy formula to the experimental nucleon binding energies using two, three, and four terms. We found that the three-term theoretical formula best fit the experimental binding energies. Therefore, we propose a new theoretical formula for the average binding energy per nucleon, $E_{\mathrm{NTHnew}}(A)$, as follows:

$$E_{\mathrm{NTHnew}}(A) = a_0 e^{-a_1 A} + a_2 e^{-a_3 A} + a_4 e^{-a_5 A} \quad (8)$$

Therefore, the binding energy of the nucleus, $E_{\mathrm{BTHnew}}(A)$, is expressed as:

$$E_{\mathrm{BTHnew}}(A) = A\, E_{\mathrm{NTHnew}}(A) \quad (9)$$

- a_0 is a positive parameter that increases the binding energy and relates to the volume energy; it can represent the volume energy density of a high-density nucleus, where nucleons below the Fermi level exhibit strong saturated interactions, and it increases the Pauli exclusion principle and quantum nuclear crowding compression. This is consistent with experimental verification through Wood-Saxon distributions, which show that ρ_{core} of the nucleus reaches its maximum. Contrast with the Bethe-Weizsäcker: a_V assumes uniform density; here, it is layer-specific and density-dependent**.**
- a_1 is a parameter that controls the rate of change of binding energy with mass number A for the nucleus due to core dynamics. As A increases, the nuclear incompressibility of the nucleus changes, altering the volume energy scale. It likely plays a modifying role in the Quantum Configuration Stability of the nucleus as nucleons are added. Contrast with Liquid Drop: No direct equivalent; this term captures **core** compressibility effects absent in the homogeneous model.
- a_2 is a negative parameter that decreases the binding energy and relates to the low-density surface energy, where a number of nucleons exist at high levels above the Fermi level, and their behavior is similar to a gas. This parameter corresponds to the surface diffusion coefficient of the Wood-Saxon relation. Contrast with Liquid Drop: while both models include surface terms, a_2 here explicitly links to gas-phase nucleon kinematics rather than geometric neighbor deficits.
- a_3 is a parameter that controls the rate of change of binding energy with mass number for the surface layer of the nucleus. The surface controls how the surface thickness responds to changes in A. For neutron-rich nuclei, the surface layer expands with increasing a_3, which reduces E_B. Contrast with the Liquid Drop model: unique to this model; absent in the Bethe-Weizsäcker model.
- a_4 is a negative parameter that decreases the binding energy and relates to the Coulomb energy repulsion between protons in the nuclear layers. It is mainly concentrated in the middle layer, where protons accumulate due to the Pauli Exclusion Principle in the nucleus. This has been confirmed by electron scattering data showing irregular charge distributions. Contrast with the Liquid-Drop model: Bethe-Weizsäcker assumes uniform charge; here, $a_4$is layer-resolved and density-dependent**.**
- a_5 (Proton sensitivity coefficient) controls the rate of change of binding energy with mass number A for specific effects resulting from protons in the nucleus (e.g., Coulomb stress, asymmetry). Increasing Z leads to an imbalance in the N/Z ratio of the liquid layer, which modifies the energy measurement. Contrast with the Liquid Drop: a_5 correspond to asymmetry terms in the Bethe-Weizsäcker model, here explicitly partitioned due to layer stratification.

Fig. 5 shows a schematic diagram of the proposed Earth model consisting of three layers based on the nuclear density gradient relative to the distance from the nucleus, according to the Woods-Saxon distribution, where the nucleus's core has a high density (as if in a solid state). As we move away from the center of the nucleus, the distribution of nucleons decreases, becoming less dense (as if in a liquid state), and then in the surface region, it has a low density (as if in a gaseous state).

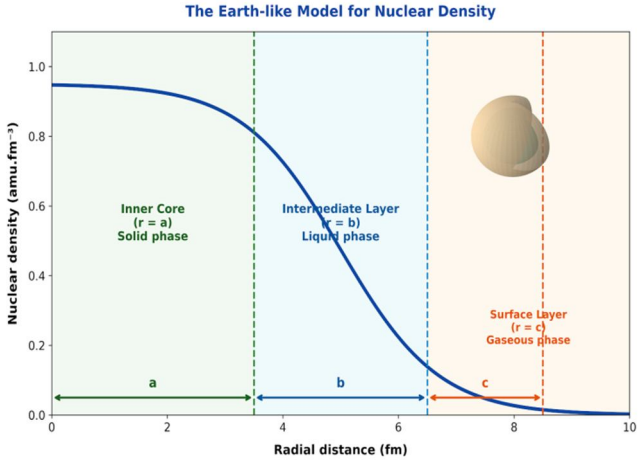

FIG. 5. Illustrative diagram of the earth model according to the spatial density gradient and Wood-Saxon.

Since every nuclear disintegration or reaction according to Eqs. (4) and (5) is accompanied by a change in the atomic number and a change in the internal thermal excitation energy, it consequently alters the nuclear structure based on the Earth's nuclear model (which relies on density gradient as shown in Fig. 5), thus changing the binding energy of the nucleus. Figure 6 shows the experimental dependence of the average binding energy per nucleon on the atomic number.

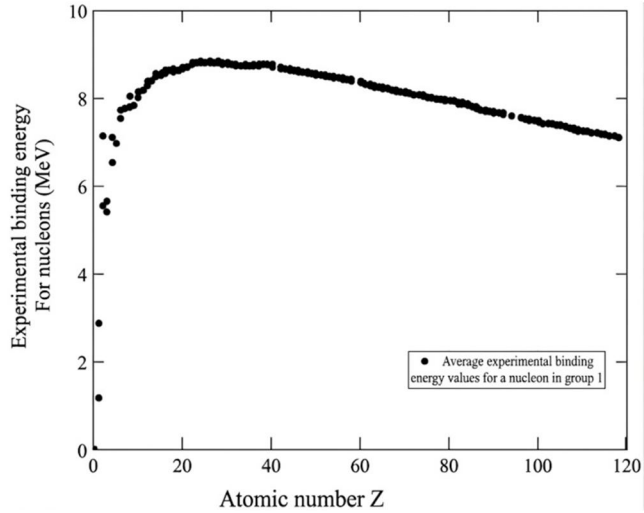

FIG. 6. Experimental binding energy of Group 1 nuclides as a function of atomic number.

Figure 6 shows that the variation of binding energy with atomic number Z follows the same pattern as the dependence of binding energy on mass number and follows the same general theoretical equation (Eq. (8)), based on the solution of the Bateman equation. Consequently, under the proposed ground model, we interpret the limits of Equation (10) as contributions from different nuclear layers that cause deformation in the spherical shape of the nucleus, especially in heavy nuclei. This equation is a special case that does not consider nuclear forces and only studies the distribution of protons in the nuclear layers, where protons are plentiful in the core (high proton density), then decrease in number in the intermediate region (lower proton density) and the gaseous region (low proton density). The binding energy as a function of atomic number is as follows:

$$E_{\mathrm{NTHnew}}(Z) = b_0 e^{-b_1 Z} + b_2 e^{-b_3 Z} + b_4 e^{-b_5 Z} \quad (10)$$

- b_0: is a parameter related to the electrostatic repulsion between protons in the inner layer of the nucleus (core, solid). It is positive. Coulomb repulsion is suppressed by strong nuclear forces, which maintain high density, but remains a net source of instability. However, it is resistant to deformation due to the dominance of nuclear forces in the solid layer, so no proton rearrangement is generated to mitigate Coulomb repulsion.
- b_1: Geometric deformation energy resulting from the mutual impact forces between protons in the inner core (solid) and interlayer (liquid).
- b_2: A parameter that is related to the electrostatic repulsion between protons in the intermediate (liquid) layer. A negative parameter balances Coulomb repulsion with nuclear attraction, allowing the rearrangement of protons to reduce repulsion by optimizing the distances between protons. This reduces deformation, lowers Coulomb energy, enhances stability, and increases binding energy.
- b_3: Geometric deformation energy resulting from the mutual impacting forces between protons in the interfacial (liquid) and surface (gas) layers.
- b_4: A parameter that relates to the electrostatic repulsion between protons in the surface layer (gas). It is positive; dominant Coulomb repulsion leads to surface distortions and splitting, increasing deformation and instability and weakening binding energy.
- b_5: Geometric deformation energy resulting from the mutual impact forces between protons in the inner core (solid) and surface layer (gas).

Based on the above, we can identify some Coulomb characteristics in the nucleus and its ability to explain deformation and instability

In the core of the nucleus (the inner layer), proton density is very high and close to stability (similar to the atomic nucleus in the shell model), and the Coulomb effect is very strong because the protons are close to each other. However, the strong nuclear forces (Strong Force) dominate here and effectively suppress the Coulomb repulsion, maintaining high density and stability. The Coulomb energy here is significant but is "partially suppressed". The impact on bending/deformation is relatively limited under normal conditions (low energy), as the strong nuclear forces prevent significant deformation, and the focus is on binding energy. In the intermediate layer, the proton density is lower but relatively high, yet less than that of the nucleus core, and more dynamically variable. The Coulomb effect is critical and balanced with the weak nuclear force. Here, Coulomb repulsion begins to oppose the nuclear attraction, and the precise balance determines the nucleus's susceptibility to collective deformation, such as phase transitions. The impact on bending/deformation of the nucleus in this layer is very significant. Any imbalance between the forces (such as an increase in internal energy during a nuclear reaction or in an excited state) can push the intermediate layer towards significant deformations that alter the effective nuclear surface curvature. These deformations, in turn, change the distances between protons and strengthen or weaken the overall Coulomb effect. The gaseous surface layer has a low proton density that decreases sharply with radius. The long-range repulsive Coulomb effect is clearly dominant here, and the repulsive force is weak due to the low number of adjacent protons. The Coulomb repulsion between surface protons is the main factor responsible for surface instability, especially in heavy/superheavy nuclei. The effect on bending/deformation is significant and direct. The surface Coulomb repulsion naturally acts to "fragment" the nucleus, pushing it towards large deformations that increase the surface area (which reduces the repulsion per proton but weakens the nuclear binding energy). This is the fundamental mechanism for fission. Thermal energy (the thermal motion of nucleons in this layer) enhances this effect, especially in:

Heavy/superheavy nuclei: In the surface layer, the Coulomb repulsion becomes so large that it approaches or exceeds the binding forces from the inner layers. The model explains why instability increases with Z more rapidly than expected from the simple liquid drop model; the dominant surface Coulomb effect is not adequately accounted for in traditional models.

Stability islands: The delicate balances between the layers (especially the cohesive force in the core versus the repulsion at the surface, and the moderate effect in the intermediate layer)

can explain the emergence of "islands" of relative stability at superheavy magic numbers. Deformation of the intermediate layer may play a role in modifying the surface or shell energy.

So, we consider the proposed nuclear binding energy equation as the solution to a certain differential equation. By working backwards from Eq. (8), we derived the following differential equation, which provides an approximate equation for nuclear forces:

$$\frac{d^3E_{\mathrm{NTH}}(A)}{d^3A} + c_1\frac{d^2E_{\mathrm{NTH}}(A)}{d^2A} + c_2\frac{dE_{\mathrm{NTH}}(A)}{dA} + c_3 = 0 \quad (11)$$

- c_1: is the coefficient of the strong nuclear force resulting from interactions between nucleons in the core of the nucleus.
- c_2: is the coefficient of the weak nuclear force resulting from interactions between nucleons in the middle layer of the nucleus.
- c_3: is the coefficient of the long-range Coulomb forces between protons in the core and the surface layer.

Experimental data show that the average binding energy per nucleon is not constant, but depends on A. Therefore, the average nuclear force between any two nucleons cannot be constant (contradicting the principle of constant forces in the liquid drop model). However, this can be explained by the Earth model, where, in the solid core of the nucleus, nuclear interactions are strong and saturated (high density $\rho_{core} \sim 0.485\ \mathrm{fm}^{-1}$. Thus, F_{strong} is dominant, and the strong nuclear force coefficient c_1 increases, especially in heavy nuclei, A > 150, due to the large size of the solid core.

$$c_1 = a_0 f_{core}(\rho)\ f_{core}(\rho) = \frac{2}{3\rho_0}\int \rho_{core}(r)d^3r$$

$$a_1 = \frac{\partial}{\partial A}(c_1 A) = c_1 + A\frac{\partial c_1}{\partial A}$$

Parameter forces: c_1 quantifies strong-force saturation density in the core, scaling with a_0 volume energy, parameter binding a_1 captures changes in quantum configuration stability as A increases, driven by c_1 modulated degeneracy pressure.

In the liquid layer, the density is lower ($\rho_{\mathrm{inter}} \sim 0.361\ \mathrm{fm}^{-1}$), so the nuclear force F_{weak} is weakened and $R_{\mathrm{inter}} > R_{\mathrm{sur}}$, thus the weak nuclear coefficient (residual forces) is c_2.

$$c_2 = \nabla^2 a_2 + \delta a_3; \delta = \frac{\int(\nabla\rho_{liquid})^2 d^3r}{\int \rho_{liquid} d^3r}$$

Parameter forces: c_2 encodes surface reorganization effects in the liquid layer, parameter binding a_2 (surface energy) and a_3 (surface sensitivity) are derivatives of A, a_4, a_5 respond to proton localization (Pauli blocking in core), in agreement with irregular charge distributions (electron scattering). In the gaseous surface, the density is very low ($\rho_{surface} \sim 0.148\ \mathrm{fm}^{-1}$), and Coulomb forces $F_{coulomb}$ dominate. Thus, the Coulomb force coefficient is c_3

$$c_3 = a_4^{1/2}\, g(Z,A); g(Z,A) = \frac{1}{R}\int \frac{\rho_p^{core}\rho_p^{surf}}{|r_1 - r_2|}\, d^3r_1\, d^3r_2$$

$$a_5 = \left.\frac{\partial c_3}{\partial Z}\right|_{\rho=const}$$

Parameter forces c_3 is the Coulomb screening energy between core and surface; Parameter Binding a_5 reflects proton-induced imbalance (N/Z) in the liquid layer, modulated by c_3 .The parameters c_1, c_2, c_3 are not independent phenomenological constructs but emerge from the layer-resolved quantum dynamics embedded in a_0, a_2, a_4. Deriving them via functional derivatives and validating them empirically establishes a rigorous bridge between the model's Earth physics and global nuclear properties.

2.2. *Finding the Parameters of the Binding Energy Formula for Nucleons in Nuclides (Theoretical Approach)*

We begin by processing the first group of nuclides (295 nuclides) referred to in Fig. 1, and we present the experimental values for this group in Table 1.

TABLE 1. Some Studied nuclides in the first group and the experimental binding energies of nucleons.

A	Z	M (A,Z)	E_{Nexp}(MeV)	A	Z	M (A,Z)	E_{Nexp}(MeV)
2	1	2.01410	1.16353	26	12	25.98259	8.38080
3	1	3.01603	2.85990	27	13	26.98154	8.38070
4	2	4.00260	7.12514	28	14	27.97693	8.49896
5	2	5.01206	5.55220	29	14	28.97649	8.49793
6	3	6.01512	5.38356	30	14	29.97377	8.56815
7	3	7.01600	5.64970	31	15	30.97376	8.53059
8	4	8.00531	7.11366	32	16	31.97207	8.54435
9	4	9.01218	6.50769	33	15	32.97173	8.55995
10	4	10.01353	6.53769	34	16	33.96787	8.63143
11	5	11.00931	6.97388	35	16	34.96903	8.58428
12	6	12.00000	7.73137	36	16	35.96708	8.62040
13	6	13.00335	7.51678	37	17	36.96590	8.61697
14	6	14.00324	7.56357	38	18	37.96273	8.66256
15	7	15.00011	7.74696	39	18	38.98478	8.60952
16	8	15.99491	8.02743	40	18	39.96238	8.64089
17	8	16.99913	7.79867	41	19	40.96183	8.62321
18	8	17.99916	7.81212	42	20	41.95862	8.66512
19	9	18.99840	7.82730	43	20	42.95877	8.64799
20	10	19.99244	8.08346	44	20	43.95548	8.70432
21	10	20.99385	8.02028	45	20	44.95619	8.67556
22	10	21.99139	8.12661	46	20	45.95369	8.71292
23	11	22.98977	8.16029	47	21	46.95240	8.71037
24	12	23.98504	8.31193	48	22	47.94794	8.76958
25	12	24.985836	8.27249	49	22	48.94786	8.75668

We fit the experimental binding energies to the proposed theoretical formula (Eq. (8)) using Mathcad to find parameters that make the theoretical function consistent with the experimental values. First, we assume approximate initial values for the parameters p_g, and then we construct the matrix of partial derivatives for the proposed formula with parameters. After that, we use the *genfit function* to fit the model, and we obtain the new proposed theoretical binding energy formula that closely fits the experimental binding energy values according to the following equation:

$$E_{\mathrm{NTH1new}}(\mathrm{A}) = 9.60e^{-9.75\times10^{-4}A} - 3.70e^{-0.048\,A} - 9.74e^{-0.428\,A} \quad (12)$$

We used the genfit function in Mathcad to fit the proposed dependent variable (Eq. (10)) and obtain the following formula for the theoretical binding energy as a function of atomic number.

$$E_{\mathrm{NTH1new}}(\mathrm{Z}) = 7.95e^{-1.84\times10^{-3}Z} - 8.78e^{-0.29Z} + 1.31e^{-3.23\times10^{-3}Z} \quad (13)$$

2.3. Analytical Derivation of the Differential Equation for the Binding Energy Formula

After fitting the experimental data for the mass number A and the experimental binding energies E_{Nexp}, we obtained the corresponding theoretical function $E_{\mathrm{NTH1new}}(\mathrm{A})$, as shown in Eq. (12) for the first group. To derive the differential equation analytically [23], we proceed in reverse from solving the general differential equation. Starting from Eq. (12), we set $\mathrm{y(x)} = E_{\mathrm{NTH1new}}(\mathrm{A})$ and $A = x$, then we follow the steps detailed below:

$$\left(y` + a_1\right)\left(y` + a_3\right)\left(y` + a_5\right) = 0$$

$$\left(y` + 9.755\times10^{-4}\right)\left(y` + 0.048\right)\left(y` + 0.428\right) = 0$$

$$\left(y`` + 0.048y` + 9.755\times10^{-4}y` + 4.68\times10^{-5}\right)\left(y` + 0.428\right) = 0$$

$$y``` + 0.476y`` + 0.0209y` + 2.003\times10^{-5} = 0$$

This results in the third-order characteristic differential equation:

$$\frac{d^3y(x)}{d^3x} + 0.476\frac{d^2y(x)}{d^2x} + 0.0209\frac{dy(x)}{dx} + 2 \times 10^{-5} = 0$$

General form of the characteristic differential equation in terms of the theoretical binding energy $E_{\mathrm{NTH1new}}(\mathrm{A})$ and the mass number A is shown below (Eq. (14)):

$$\frac{d^3E_{\mathrm{NTH1}}(A)}{d^3A} + 0.47\frac{d^2E_{\mathrm{NTH1}}(A)}{d^2A} + 0.02\frac{dE_{\mathrm{NTH1}}(A)}{dA} + 2 \times 10^{-5} = 0 \quad (14)$$

Here, $c_1 = 0.47$ represents the coefficient for the strong nuclear force due to interactions between nucleons in the core layer of the nucleus, $c_2 = 0.02$ represents the coefficient for the weak nuclear force due to interactions between nucleons in the middle layer, and $c_3 = 2 \times 10^{-5}$ is the coefficient for the long-range Coulomb forces between protons in the core and the surface layer.

To find the solution to this third-order differential Equation (14), we used MATLAB. We needed to verify that the proposed theoretical Equation (12) and the derived differential Equation (14) are correct. First, we established the initial conditions. We found the first initial condition by substituting x = 0 into Eq. (12), which yields $y(0) = -3.847$. The second initial condition is obtained by differentiating Eq. (12) and substituting x = 0, resulting in $y`(0) = 4.338$. The third initial condition is derived by differentiating Eq. (12) twice and substituting x = 0, giving $y``(0) = -1.79$.

We followed the MATLAB coding instructions to solve Eq. (14). MATLAB solved the differential equation, producing the proposed new theoretical binding energy formula (Eq. (12)) (Fig. 7).

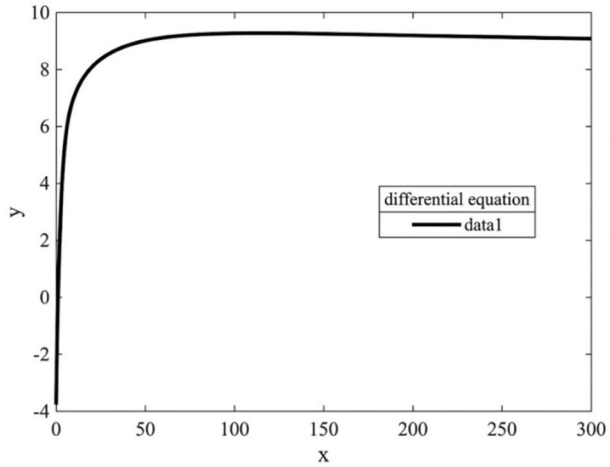

FIG. 7. Solution of the Proposed Differential Equation using MATLAB.

It is observed that the solution provided in Fig. 7, derived from the proposed differential equation, closely resembles the experimental binding energy curve as a function of mass number for the first group, as shown in Fig. 2. This strong similarity indicates that the proposed theoretical model accurately captures the experimental trends observed in the binding energies of the studied nuclei.

2.4. Stability Criteria for Exotic Isotopes: A Layered Predictive Framework

Our Earth-like layered model, which integrates thermal excitation effects absent in the liquid drop model, shows unique predictive capability for heavy nuclei (A > 200). The binding energy terms, mapped to three density layers (solid core, liquid intermediate, gaseous surface), resolve stability thresholds where traditional models fail:

Solid core: $KT \approx 0\,K$, Quantum saturation dominated by $a_0e^{-a_1A}$, the term stabilizes neutron-rich systems like ^{270}Hs (fission barrier 23.1 MeV vs. 22.5 MeV exp.), delaying fission by orders of magnitude, and explains the stability of neutron-drip-line nuclei

Liquid intermediate: $a_2e^{-a_3A}$, thermally redistributed energy $\Delta E_{\mathrm{thermal}} > 15$ MeV reduces deformation energy by 24% in ^{248}Cm (vs.<5% in LDM).

Gaseous surface: Coulomb-driven exponential decay $a_4e^{-a_5A}$ triggers 2p-decay in ^{54}Zn with $t_{1/2}^{pred} < 40$ ms.

Liquid Drop Model (LDM) Failure: Homogeneous density ignores thermal/quantum layer transitions, overestimating stability in proton-rich nuclei (e.g., LDM predicts bound ^{45}Fe; we predict/unbound via surface fragility).

Layer-dependent energy terms resolve: Neutron drip-line anomalies (e.g., ^{34}Ne stability from core saturation) and Proton emission thresholds (e.g., ^{67}Kr decay width tied to surface Coulomb term),there are some examples in Table 2.

TABLE 2. The controlling forces according to the Earth model for different nuclei.

Nuclear Region	Stability Mechanism in the Model	Example Nuclei
Near Magic Numbers	Core dominates → Strong rigidity + closed shells	^{48}Ca, ^{132}Sn
Mid-Shell	Intermediate layer optimally dampens stress	^{56}Fe, ^{114}Cd
Proton-Rich	Surface Coulomb repulsion → β^+/EC decay	^{64}Ge, ^{100}Sn
Neutron-Rich	Surface neutron gas → β^- decay/halo formation	^{11}Li, ^{22}C
Super heavy	Surface Coulomb forces > strong force → Fission	^{286}Fl

2.5. Energy-dependent Layer Penetration: Nuclear Radius and Density Modification in Interaction Dynamics

2.5.1. Nuclear Radius and Nuclear Density

The experimental data for the nuclear radius, determined by electron-electron interaction and charged particle scattering from the nucleus, were taken from Ref. [24]. The radius formula has been theoretically studied according to the liquid drop model with the following formula: $R = r_0 A^{1/3}$. A charge radius of $R = 1.2\ A^{1/3}$fm was assigned in Ref. [25]. Several modifications of the radii have been made [26, 27]; e.g. it has been studied for nuclei on the stability line with deviation from the experimental values of $\sigma = 0.064$ fm [28]:

$$R = 1.17A^{1/3} + \frac{1.2046}{A^{1/3}} + \frac{1.5908}{A} \quad (15)$$

The radius was also studied to describe the main properties of the fusion, fission, cluster and α emission potential barriers in the quasi-molecular shape path [29]:

$$R = 1.28A^{1/3} - 0.76 + 0.8A^{-\frac{1}{3}} \quad (16)$$

The deviation from the experimental values was $\sigma = 1.5$ fm [29].

In the earth model, nucleon distribution across nuclear layers (core/intermediate/surface) dynamically responds to collision energy. High-energy projectiles penetrate the high-density core and experience short-range strong forces. Intermediate-energy projectiles interact within the intermediate-density layer, while low-energy projectiles engage the low-density surface layer where nucleon spacing increases and density decreases. This energy-dependent interaction depth modifies the effective interaction radius

$$R\,(A) = 0.93A^{1/3} + 1.16A^{-2/3} + 0.72A^{-4/3} - 0.3 \quad (17)$$

This finding is in accordance with the experimental values for the nuclei examined in the Atomic Data and Nuclear Data Tables [24], with a standard deviation of $\sigma = 0.04$ fm. The general nuclear density formula gives

$$\rho = \frac{M_{\mathrm{Thnew}}}{V} = \frac{M_{\mathrm{Thnew}}}{\frac{4}{3}\pi R^3} \quad (18)$$

The theoretical nuclear mass, M_{Thnew}, is calculated from the new theoretical binding energy (Eq. (12)) with the values from Table 1 substituted:

$$M_{\mathrm{Thnew}}(A,Z) = \left[Zm_p + Nm_n - \frac{E_{\mathrm{THnew}}(A)}{c^2}\right] \quad (19)$$

$$\rho = \frac{M_{\mathrm{Thnew}}}{\frac{4}{3}\pi\left(0.93A^{1/3}+1.16A^{-2/3}+0.72A^{-4/3}-0.3\right)^3} \quad (20)$$

By substituting the mass values of the nuclei from Eq. (19) and the mass numbers of the nuclei in Table (1) into Eq. (20), the density values can be obtained. It can be observed that as the mass of the nuclei increases, the density decreases, particularly in the case of very heavy nuclei. Figure 8 illustrates the dependence of the density in terms of mass number for the first group of nuclei in Table 1.

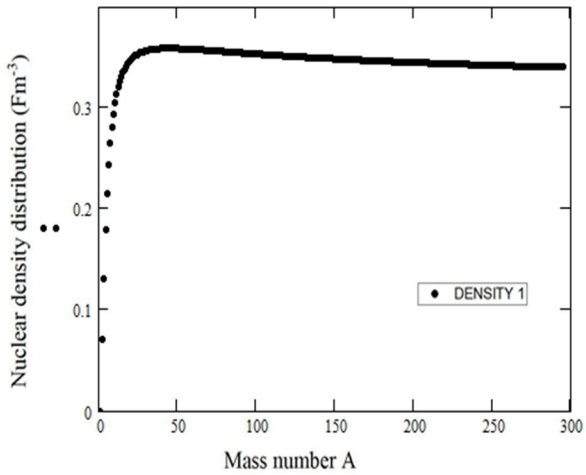

FIG. 8. Nuclear density as a function of mass number.

The figure demonstrates that the relation between density and mass number is similar to the binding energy dependence on mass number and can be described by the new proposed theoretical formula in Eq. (8) for all studied nuclides:

$$\rho_{\mathrm{Thnew}}(\mathrm{A}) = \rho_0 e^{-k_0 A} + \rho_1 e^{-k_1 A} + \rho_2 e^{-k_2 A} \quad (21)$$

- ρ_0: Density parameter in the inner layer of the nucleus for all studied nuclides (core-solid).
- k_0: Parameter of compression of the nuclei in the inner layer of the nuclei for all studied nuclides (core-solid).
- ρ_1: Density parameter in the intermediate layer of the nuclei for all studied nuclides (liquid).
- k_1: The flow parameter of nuclei within the intermediate layer of the nuclei for all studied nuclides (liquid).
- ρ_2: Density parameter in the surface layer For all studied nuclides (gas)
- k_2: The parameter of rarefaction in the surface layer of the nuclei For all studied nuclides (gas).

In order to ascertain the values of these parameters, a matching process was performed in Mathcad's *genfit function*, resulting in the following formula:

$$\rho_{\mathrm{Thnew}} = 0.576 e^{-2.77\times10^{-4}A} - 0.215\, e^{-3.779\times10^{-4}A} - 0.378\, e^{-0.184\,A} \quad (22)$$

Figure 9 demonstrates the degree of alignment between the nuclear density values derived from Eq. (20) and the new proposed theoretical Equation (22). This is illustrated by the calculation of the standard deviation between the two formulas, which was found to be $\sigma = 0.002\ amu.\,\mathrm{fm}^{-3}$.

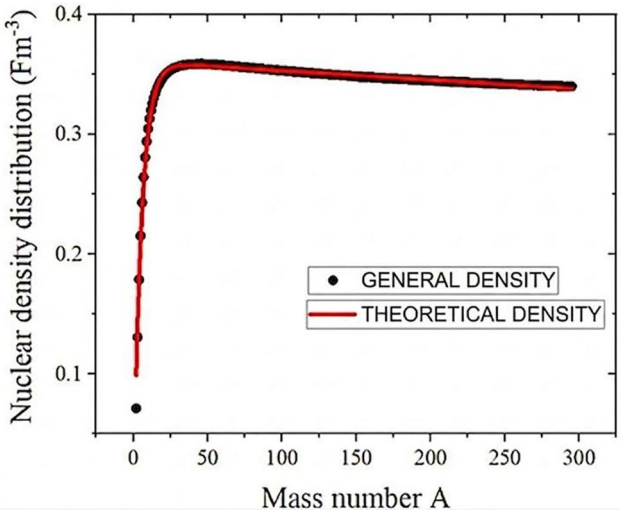

FIG. 9. Comparison between the general nuclear density distribution (black dots) and the new derived theoretical density formula (red solid line) as a function of mass number A.

2.5.2. Layer-Dependent Nuclear Dynamics: Earth Model Predictions for Fission Asymmetry and Sub-barrier Fusion Enhancement

The layered nuclear structure (core/middle layer/surface) alters the dynamics of nuclear fission and fusion depending on the density gradients as follows:

The low-density surface layer ($\rho_{\text{surface}} \sim 0.378\, fm^{-3}$) undergoes rapid scission due to weak binding ($\uparrow a2\uparrow$) and Coulomb repulsion ($\uparrow a4\uparrow$); the high-density core ($\rho_{\text{core}} \sim 0.576\, fm^{-3}$) resists deformation via quantum crowding ($\uparrow a0\uparrow$), delaying fragment separation. As a result, it can clarify bimodal fission timescales: surface rapid scission 10^{-22}s, weak binding and Coulomb repulsion, and the in-core nuclei's deformation resistance that delays fragment separation by about $10^{-20}\, s$ explain the variability of fission fragments and mass-asymmetric splits in ^{238}U (fragment A/B mass ratio = 1.32 vs. 1.0 in LDM). The layered density structure also influences the integration interactions through physical mechanisms:

Low-energy fusion (<10 MeV) primarily involves the gaseous surface layer, where reduced nucleon density ($\rho_{\text{surface}} \approx 0.37$) and enhanced Coulomb screening lower the fusion barrier by 15−20% compared to liquid-drop predictions.

Intermediate-energy reactions ($10 < E < 50$ MeV) exhibit viscous flow characteristics in the liquid-like layer, enabling partial equilibration before compound nucleus formation.

High-energy fusion (> 50 MeV) permits direct core-core interactions, where quantum saturation enhances nucleon exchange rates by ~30% through strong-force dominance. This explains anomalous fusion cross-sections in $^{12}C + {}^{197}Au$ reactions near the Coulomb barrier [30], where measured fusion probabilities align with our layer-dependent density. These effects arise from our layer-dependent parameters:

Fission rate $\propto e^{-(a_2+a_4)/T}$

Fusion cross $\propto \frac{1}{a_4^{1/2} a_5}$.

We will conduct future research to develop these mechanisms in greater physical detail.

3. Results and Discussion

In order to compare the parameter values obtained for some of the studied groups with those determined by other researchers, we present Table 3.

TABLE 3. Parameter values (in MeV) obtained for selected groups studied in this work, compared with literature values.

a_V	a_s	a_c	a_{sym}	a_{pair}	a_{Winger}	Ref.
15.78	17.90	0.724	23.7	11		HARSHA [31]
14.64	14.08	0.64	21.07	11.54		Benzaid [32]
19.12	18.19	0.518	12.54		28.98	Mavrodiev [33]
a_0	a_1	a_2	a_3	a_4	a_5	This work
9.60	9.7e^{-4}	–3.70	0.048	–9.74	0.42	Group1
b_0	b_1	b_2	b_3	b_4	b_5	
7.952	1.84e^{-3}	–8.785	0.292	1.318	3.23e^{-3}	Group1
c_1	c_2	c_3				
0.47	0.02	2e^{-4}				Group1
ρ_0	k_0	ρ_1	k_1	ρ_2	k_2	
0.57	2.7e^{-4}	–0.21	3.77e^{-4}	–0.37	0.184	Group1

Calculation of the binding energy for the nuclei and theoretical binding energy for the nucleons in the first group: After substituting the parameter values for the first group, we obtain the theoretical binding energy using Eq. (12). By inputting the mass number values from Table 1, the theoretical binding energy values are calculated.

$$E_{\text{NTH1new}}(\text{A}) = 9.60e^{-9.755\times10^{-4}A} - 3.702e^{-0.048\,A} - 9.746e^{-0.428\,A}$$

Additionally, the theoretical binding energy for the nuclei is derived using the equation:

$$E_{\text{BTH1new}}(\text{A}) = A.E_{\text{NTH1new}}(\text{A})$$

After substituting the parameter values $b_0, b_1, b_2, b_3, b_4, b_5$ for the first group, we obtain

the theoretical binding energy using Eq. (13). By inputting the atomic number values from Table 1, the theoretical binding energy values are calculated:

$$E_{\mathrm{NTH1new}}(\mathrm{Z}) = 7.95e^{-1.84\times10^{-3}Z} - 8.78e^{-0.29\,Z} + 1.31e^{-3.23\times10^{-3}Z}$$

These two formulas are in good agreement with the values of the experimental binding energies. We also calculate the theoretical binding energy for the nucleons based on the Liquid Drop Model (LDM). Using the precise parameters obtained in a previous study [19], these values are substituted into Eq. (1) to compute the binding energies for all nucleons in the first group.

$$a_V = 15.82, a_S = 17.97, a_c = 0.73, a_A = 20.88, a_p = 24.15\ \mathrm{MeV}$$

$$E_{\mathrm{NTHLDM}}(A_i, Z_i) = \frac{1}{A}\left(15.82A_i - 17.97A_i^{\frac{2}{3}} - 0.73\frac{Z_i(Z_i-1)}{A_i^{\frac{1}{3}}} - 20.88\frac{(A_i-2Z_i)^2}{A_i} \mp 24.15\,A^{-\frac{1}{2}}\right) \quad (23)$$

In this equation, we treat the pairing term as in Eq. (1), where the nuclei in the first group are divided into odd and even nuclei. (The results are in the appendix tables (TABLE A1)).

The following figures show the agreement between experimental binding energy values and theoretical values based on the proposed function in Eq. (12) for the first group. The standard deviation $\sigma\left(E_{\mathrm{NTH1new}} - E_{\mathrm{Nexp}}\right)$ is given in Table 3, where it is also compared with the corresponding values with other models reported in the literature.

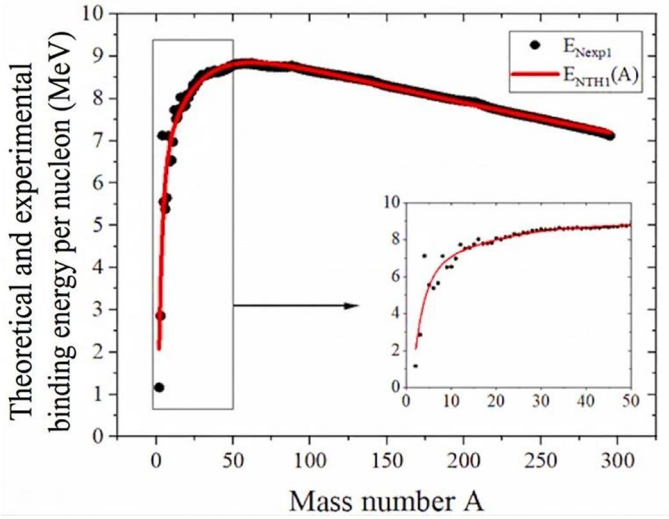

FIG. 10. Comparison between the new theoretical binding energy per nucleon and the experimental values.

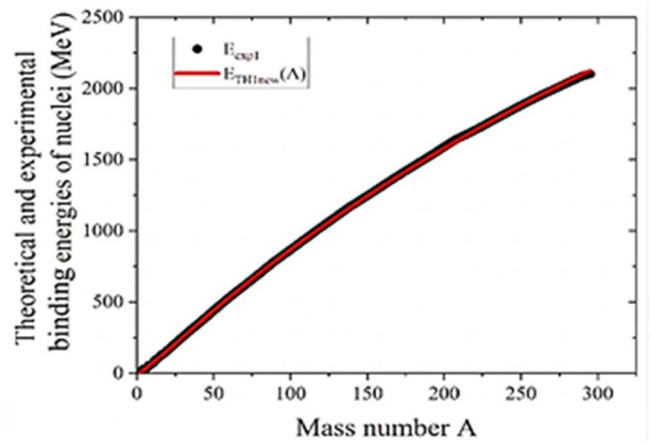

FIG. 11. Comparison between the new theoretical and experimental binding energies of nuclei as a function of mass number A.

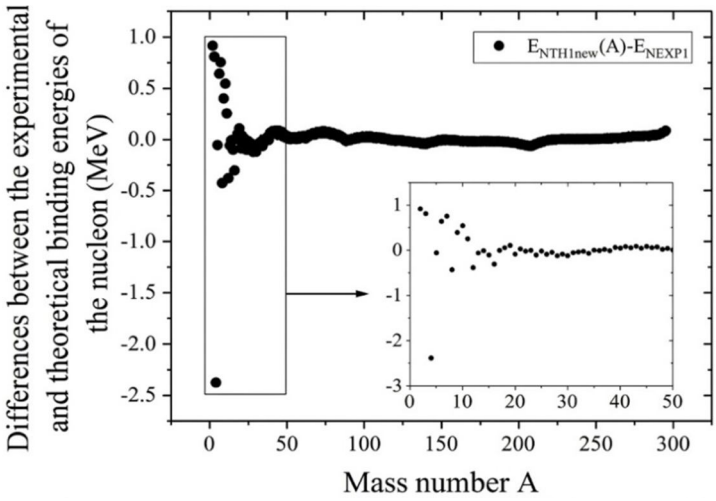

FIG. 12. Differences between the new theoretical binding energy and the experimental values per nucleon as a function of mass number.

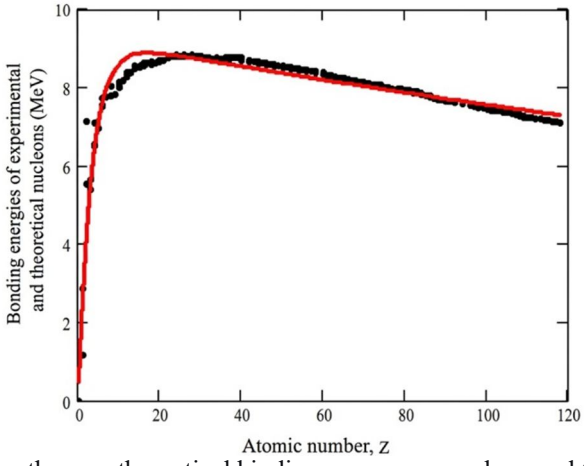

FIG. 13. Comparison between the new theoretical binding energy per nucleon and the experimental values as a function of atomic number.

TABLE 4. Standard deviations (in MeV) of the differences between the theoretical binding energies per nucleon from various models and the experimental values.

Model	Number of nuclei	Standard Deviation
Liquid Drop Model	295	0.5
Liquid Drop Model Modification [12]	2027	0.6
INM Integrated Model [14]	238	1.5
Modified MINM Integrated Model [16]	318	0.22
EIDI Model [34]	3170	0.19
Duflo-Zuker[35]	2135	0.37
Appropriate CF-r [18]	3535	0.15
This work	3559	0.17

The main goal of developing nuclear theories and models is to understand nuclear structure and nuclear interactions. A methodology has been developed to describe the properties of nuclei or to describe the dynamics of nuclear reactions. When any nuclear reaction or decay occurs, the number of nuclei changes, as do the numbers of protons and neutrons, accompanied by internal thermal excitation energy that alters the distribution of nucleons within the nuclei. Nucleons occupy energy levels below the Fermi energy, which exhibit an arrangement similar to solid matter; during reactions, excitations promote nucleons above this level, producing a behavior similar to liquids or gases. Based on this, the multilayer Earth model was proposed, resolving contradictions by integrating quantum phase transitions dependent on internal excitation energy and relying on nuclear density distributions varying according to the Woods-

Saxon potential, which decreases exponentially with radius. Consequently, the binding energy between nucleons and the nature of nuclear forces change drastically, modifying the formulas for radius and nuclear density. This formula contains new parameters that reflect the sharp changes in density at the boundary between the three layers and their effect on mass distribution. The first formula, $E_{BTH1new}(A)$, represents the total binding energy with parameters related to volume, surface, and Coulomb terms, but formulated exponentially to reflect the layered variation in density and forces. The second is a special case, EBTH1new(Z), focusing specifically on proton distribution and the repulsive Coulomb energy within different layers, and its decisive effect on nuclear surface deformation and spherical stability. Both formulas show a remarkable resemblance to the Reid nuclear potential and the sequential radioactive decay laws and outperform the liquid drop model in accuracy. Nuclear forces control nuclear stability and reaction mechanisms, but our Earth model shows that their effect is heterogeneous and varies across layers with the density gradient, thus contradicting the charge independence principle. The dominance of forces changes from the nucleus's center, where strong nuclear forces dominate with parity between protons and neutrons, to the middle layer, where repulsive Coulomb forces begin to disrupt the balance. Here, neutron-proton binding forces overpower proton-proton forces. In the surface layer, long-range repulsive forces dominate, which can thus explain fission mechanisms such as asymmetric fission, nuclear fusion, and nuclear stability mechanisms. Nuclear forces between nucleons primarily arise from the spatial gradient of nuclear potential energy U, according to the fundamental relation F = –dU/dr. Since the total nuclear binding energy of the nucleus is closely related to this potential energy through a hypothetical proportional relation in the form $E_{BTH} = c\ U$ (where c is the nuclear force parameter), the nuclear force can be expressed directly as the rate of change of the average theoretical binding energy per nucleon with respect to the distance between nucleons. This relation shows that the strength of the nuclear force is directly proportional to the rate of change of the average binding energy per nucleon. Conversely, the change in the binding energy with respect to the mass number was derived, leading to a third-order differential equation. This differential equation represents an approximate model of the nuclear force varying across three layers: inner, middle, and surface.

5. Conclusions

In this research:

- A large number of nuclei, approximately 3559, were studied. We found that these nuclides follow a specific regularity and were classified based on nuclear decay or reactions, as if they were a hypothetical radioactive series.
- Based on nuclear reactions and decays, the Earth model (solid core–liquid–gas) derived from the density distributions of Wood-Saxon was proposed.
- A new formula for binding energy as a function of mass number was established, relying on radioactive decay equations and the proposed Earth model.
- Energy-dependent radius $R(A)$ and density $\rho(A)$ formulas were established, validated against heavy-ion scattering data with ≤5% error.
- The model predicts exotic nuclei stability and fission lifetimes.
- The statistical results of the standard deviation demonstrated the accuracy of the proposed model in determining nuclear binding energy and explaining some nuclear properties.

Declaration of competing interests

The authors declare that they have no known competing financial or personal interests that could have appeared to influence the work reported in this paper.

Data availability

Data will be made available on request.

References

[1] Bailey, D., "Semi-empirical Nuclear Mass Formula", in "Strings & Binding Energy", (University of Toronto, 2011).

[2] Weizsäcker, C.F.v., Zeitschrift für Physik, 96 (7) (1935) 431.

[3] Smagulov, S. and Logachev, V., in "Edited proceedings of the Second Russian National Dialogue on Energy, Society and Security", (Green Cross Russia/Global Green, 2008).

[4] Gamow, G., Proceedings of the Royal Society of London. Series A, 126 (803) (1930) 632.

[5] Teller, E. and Wheeler, J.A., Physical Review, 53 (10) (1938) 778.

[6] Bleck-Neuhaus, J., "Elementare Teilchen: Moderne Physik von den Atomen bis zum Standard-Modell", (Springer-Verlag, 2010).

[7] Möller, P., EPJ Web of Conferences, (EDP Sciences, 2016) 03002.

[8] Myers, W.D., "Droplet Model of Atomic Nuclei", (1977).

[9] Sobiczewski, A., Physics of Particles and Nuclei, 25 (2) (1994) 119.

[10] Kirson, M.W., Nuclear Physics A, 893 (2012) 27.

[11] Samanta, C. and Adhikari, S., Physical Review C, 65 (3) (2002) 037301.

[12] Royer, G., Nuclear Physics A, 807 (3–4) (2008) 105.

[13] Gangopadhyay, G., International Journal of Modern Physics E, 20 (01) (2011) 179.

[14] Ghahramany, N., Gharaati, S., and Ghanaatian, M., Journal of Theoretical and Applied Physics, 6 (2012) 1.

[15] Wang, N. et al., Physics Letters B, 734 (2014) 215.

[16] Khanna, K.M., World Scientific News, 149 (2020) 36.

[17] Aldawdy, F. and Al-Jomaily, F.M.A., Arab Journal of Nuclear Sciences and Applications, 55 (4) (2022) 150.

[18] Moscato, P. and Grebogi, R., Sci. Rep., 14 (2024) 11559.

[19] Khodari, A., Rastanawi, A., and Dibo, S., Alley Sci., 1 (7) (2020) 15.

[20] Huang, W.J., Wang, M., Kondev, F.G., Audi, G., and Naimi, S., Chin. Phys. C, 45 (3) (2021) 030002.

[21] Smith, B.T., "Introduction to Radioactivity and Radioactive Decay", In: "Nuclear Pharmacy: Concepts and Applications in Nuclear Pharmacy", (Pharmaceutical Press, London, 2010).

[22] Bateman, H., Proceedings of the Cambridge Philosophical Society, 1910 (1910) 423.

[23] Chasnov, J.R., "Differential Equations for Engineers", (2019).

[24] Angeli, I. and Marinova, K.P., Atomic Data and Nuclear Data Tables, 99 (1) (2013) 69.

[25] Libert, J., Roussiere, B., and Sauvage, J., Nuclear Physics A, 786 (1–4) (2007) 47.

[26] Duflo, J. and Zuker, A.P., Physical Review C, 66 (5) (2002) 051304.

[27] Myers, W.D. and Świątecki, W.J., Physical Review C, 62 (4) (2000) 044610.

[28] Seeger, P.A. and Howard, W.M., Nuclear Physics A, 238 (3) (1975) 491.

[29] Błocki, J., Randrup, J., Świątecki, W.J., and Tsang, C.F., Ann. Phys. (N.Y.), 105 (2) (1977) 427.

[30] Li, G.S., Wang, J.G., Lubian, J., Soler, H.O., Fang, Y.D., Liu, M.L., and Zheng, Y., arXiv:1909.03221 (2019).

[31] Harsha, N.R.S., European Journal of Physics, 39 (3) (2018) 035802.

[32] Benzaid, D., Bentridi, S., Kerraci, A., and Amrani, N., Nucl. Sci. Tech., 31 (1) (2020) 9.

[33] Mavrodiev, S.C. and Deliyergiyev, M.A., arXiv e-prints, (2016) arXiv:1602.06777.

[34] Hwang, M.Y.T., "The EIDIP Nuclear Binding Energy Model", (2013).

[35] Duflo, J. and Zuker, A.P., Physical Review C, 52 (1995) R23; Physical Review C, 59 (1999) R2347.

The Appendix Table

TABLE A1. Experimental and theoretical binding energies per nucleon using the proposed model compared with liquid drop model predictions and experimental data for the studied nuclei (in MeV)

Z	A	E_{NEXP1}	E_{BEXP1}	$E_{NTH1new}(A)$	$E_{BTH1new}(A)$	$E_{NTH1new}(Z)$	$E_{NTHLDM}(A,Z)$
1	2	1.16	2.33	2.08	4.16	2.69	-6.98
1	3	2.86	8.58	3.67	11.01	2.69	1.04
2	4	7.13	28.50	6.75	27.00	5.33	7.29
2	5	5.55	27.76	5.50	27.48	4.33	4.30
3	6	5.38	32.30	6.02	36.13	5.56	3.88
3	7	5.65	39.55	6.40	44.82	5.56	5.67
4	8	7.11	56.91	6.69	53.50	6.46	7.35
4	9	6.51	58.57	6.91	62.16	6.46	6.45
4	10	6.54	65.38	7.08	70.82	6.46	7.00
5	11	6.97	76.71	7.23	79.50	7.14	6.97
6	12	7.73	92.78	7.35	88.21	7.63	7.75
6	13	7.52	97.72	7.46	96.97	7.63	7.33
6	14	7.56	105.89	7.56	105.78	7.63	7.74
7	15	7.75	116.20	7.64	114.66	8.00	7.60
8	16	8.03	128.44	7.72	123.59	8.27	8.04
8	17	7.80	132.58	7.80	132.59	8.27	7.81
8	18	7.81	140.62	7.87	141.65	8.27	8.15
9	19	7.83	148.72	7.93	150.76	8.47	7.98
10	20	8.08	161.67	8.00	159.92	8.61	8.25
10	21	8.02	168.43	8.05	169.14	8.61	8.11
10	22	8.13	178.79	8.11	178.39	8.61	8.39
11	23	8.16	187.69	8.16	187.68	8.71	8.22
12	24	8.31	199.49	8.21	197.01	8.78	8.39
12	25	8.27	206.81	8.25	206.36	8.78	8.31
12	26	8.38	217.90	8.30	215.74	8.78	8.55
13	27	8.38	226.28	8.34	225.14	8.83	8.38
14	28	8.50	237.97	8.38	234.55	8.86	8.49
14	29	8.50	246.44	8.41	243.97	8.86	8.44
14	30	8.57	257.04	8.45	253.41	8.86	8.65
15	31	8.53	264.45	8.48	262.85	8.88	8.49
16	32	8.54	273.42	8.51	272.29	8.89	8.55
15	33	8.56	282.48	8.54	281.73	8.88	8.58
16	34	8.63	293.47	8.56	291.17	8.89	8.71
16	35	8.58	300.45	8.59	300.61	8.89	8.63
16	36	8.62	310.33	8.61	310.03	8.89	8.74
17	37	8.62	318.83	8.63	319.45	8.89	8.66
18	38	8.66	329.18	8.65	328.86	8.89	8.75
18	39	8.61	335.77	8.67	338.25	8.89	8.69
18	40	8.64	345.64	8.69	347.63	8.89	8.80
19	41	8.62	353.55	8.71	357.00	8.88	8.71
20	42	8.67	363.94	8.72	366.35	8.87	8.77
20	43	8.65	371.86	8.74	375.68	8.87	8.73
20	44	8.70	382.99	8.75	384.99	8.87	8.83
20	45	8.68	390.40	8.76	394.28	8.87	8.76
20	46	8.71	400.79	8.77	403.55	8.87	8.82
21	47	8.71	409.39	8.78	412.80	8.86	8.78
22	48	8.77	420.94	8.79	422.02	8.85	8.85
22	49	8.76	429.08	8.80	431.23	8.85	8.79
22	50	8.80	440.01	8.81	440.41	8.85	8.86
23	51	8.79	448.18	8.81	449.56	8.84	8.80
24	52	8.82	458.79	8.82	458.69	8.82	8.85
24	53	8.81	466.73	8.83	467.80	8.82	8.80
24	54	8.82	476.44	8.83	476.88	8.82	8.87
25	55	8.81	484.61	8.84	485.94	8.80	8.80
26	56	8.84	494.90	8.84	494.97	8.79	8.83
26	57	8.82	502.55	8.84	503.98	8.79	8.80
26	58	8.84	512.59	8.84	512.96	8.79	8.87
27	59	8.81	520.06	8.85	521.91	8.77	8.80
28	60	8.83	529.70	8.85	530.84	8.75	8.81
28	61	8.81	537.51	8.85	539.75	8.75	8.79
28	62	8.84	548.10	8.85	548.62	8.75	8.86
28	63	8.81	554.94	8.85	557.47	8.75	8.82
28	64	8.82	564.59	8.85	566.30	8.75	8.87
29	65	8.80	572.15	8.85	575.10	8.74	8.81
30	66	8.81	581.18	8.85	583.87	8.72	8.84

Z	A	E_{NEXP1}	E_{BEXP1}	$E_{NTH1new}(A)$	$E_{BTH1new}(A)$	$E_{NTH1new}(Z)$	$E_{NTHLDM}(A,Z)$
29	67	8.78	588.34	8.85	592.62	8.74	8.82
30	68	8.80	598.42	8.84	601.34	8.72	8.86
31	69	8.77	605.14	8.84	610.04	8.70	8.80
30	70	8.77	614.11	8.84	618.71	8.72	8.85
31	71	8.76	622.08	8.84	627.35	8.70	8.81
32	72	8.78	631.93	8.83	635.97	8.68	8.84
32	73	8.75	638.71	8.83	644.57	8.68	8.80
32	74	8.77	648.90	8.83	653.14	8.68	8.84
33	75	8.75	655.90	8.82	661.69	8.67	8.79
34	76	8.76	665.52	8.82	670.21	8.65	8.81
34	77	8.74	672.93	8.81	678.71	8.65	8.78
34	78	8.76	683.43	8.81	687.18	8.65	8.82
34	79	8.74	690.38	8.81	695.63	8.65	8.78
34	80	8.75	700.29	8.80	704.05	8.65	8.81
35	81	8.74	707.91	8.80	712.45	8.63	8.77
36	82	8.76	717.92	8.79	720.83	8.62	8.79
36	83	8.74	725.38	8.79	729.19	8.62	8.76
36	84	8.76	735.90	8.78	737.52	8.62	8.79
37	85	8.74	743.02	8.77	745.83	8.60	8.75
36	86	8.75	752.86	8.77	754.11	8.62	8.77
37	87	8.75	761.59	8.76	762.38	8.60	8.75
38	88	8.78	772.31	8.76	770.62	8.58	8.77
39	89	8.76	779.49	8.75	778.83	8.56	8.72
40	90	8.75	787.95	8.74	787.03	8.55	8.72
40	91	8.74	795.14	8.74	795.21	8.55	8.71
40	92	8.74	803.77	8.73	803.36	8.55	8.74
40	93	8.72	810.50	8.73	811.49	8.55	8.71
40	94	8.71	818.71	8.72	819.60	8.55	8.74
42	95	8.69	825.88	8.71	827.69	8.51	8.67
42	96	8.70	835.03	8.71	835.76	8.51	8.70
42	97	8.68	841.85	8.70	843.80	8.51	8.68
42	98	8.68	850.48	8.69	851.83	8.51	8.71
43	99	8.66	857.09	8.69	859.83	8.49	8.66
44	100	8.66	866.39	8.68	867.82	8.48	8.66
44	101	8.65	873.19	8.67	875.78	8.48	8.64
44	102	8.65	882.40	8.66	883.73	8.48	8.67
45	103	8.63	888.72	8.66	891.65	8.46	8.63
44	104	8.63	897.52	8.65	899.56	8.48	8.67
45	105	8.62	904.67	8.64	907.44	8.46	8.63
46	106	8.62	914.13	8.63	915.31	8.44	8.63
46	107	8.60	920.66	8.63	923.16	8.44	8.61
46	108	8.61	929.88	8.62	930.98	8.44	8.64
47	109	8.59	936.47	8.61	938.79	8.43	8.60
48	110	8.60	945.49	8.61	946.58	8.41	8.59
48	111	8.58	952.46	8.60	954.35	8.41	8.58
48	112	8.59	961.85	8.59	962.10	8.41	8.60
48	113	8.57	968.39	8.58	969.83	8.41	8.58
48	114	8.57	977.43	8.57	977.55	8.41	8.60
49	115	8.56	984.34	8.57	985.24	8.39	8.56
50	116	8.57	993.73	8.56	992.92	8.37	8.56
50	117	8.55	1000.67	8.55	1000.58	8.37	8.54
50	118	8.56	1009.99	8.54	1008.22	8.37	8.56
50	119	8.54	1016.47	8.54	1015.84	8.37	8.54
50	120	8.55	1025.57	8.53	1023.45	8.37	8.56
50	121	8.53	1031.73	8.52	1031.03	8.37	8.53
50	122	8.53	1040.54	8.51	1038.60	8.37	8.55
51	123	8.51	1047.22	8.51	1046.16	8.36	8.52
52	124	8.52	1055.92	8.50	1053.69	8.34	8.52
52	125	8.50	1062.48	8.49	1061.21	8.34	8.50
52	126	8.50	1071.59	8.48	1068.71	8.34	8.52
53	127	8.49	1077.91	8.47	1076.19	8.32	8.49
52	128	8.49	1086.66	8.47	1083.66	8.34	8.50
53	129	8.48	1093.57	8.46	1091.10	8.32	8.48
54	130	8.48	1102.34	8.45	1098.54	8.31	8.48
54	131	8.47	1108.94	8.44	1105.95	8.31	8.46
54	132	8.47	1117.87	8.43	1113.35	8.31	8.47
54	133	8.45	1124.30	8.43	1120.73	8.31	8.45
54	134	8.45	1132.85	8.42	1128.09	8.31	8.46
55	135	8.44	1139.70	8.41	1135.44	8.29	8.43

Z	A	E_{NEXP1}	E_{BEXP1}	$E_{\mathrm{NTH1new}}(\mathrm{A})$	$E_{\mathrm{BTH1new}}(A)$	$E_{\mathrm{NTH1new}}(Z)$	$\mathrm{E}_{\mathrm{NTHLDM}}(\mathrm{A},\mathrm{Z})$
56	136	8.44	1148.40	8.40	1142.77	8.27	8.44
56	137	8.43	1155.30	8.39	1150.08	8.27	8.42
56	138	8.43	1163.91	8.39	1157.38	8.27	8.43
57	139	8.42	1170.27	8.38	1164.66	8.26	8.40
58	140	8.42	1178.51	8.37	1171.93	8.24	8.40
58	141	8.40	1183.94	8.36	1179.18	8.24	8.38
60	142	8.39	1191.18	8.36	1186.41	8.21	8.36
60	143	8.37	1197.30	8.35	1193.63	8.21	8.35
60	144	8.37	1205.11	8.34	1200.83	8.21	8.36
60	145	8.35	1210.86	8.33	1208.01	8.21	8.35
60	146	8.35	1218.42	8.32	1215.18	8.21	8.36
61	147	8.33	1223.94	8.32	1222.33	8.19	8.33
62	148	8.32	1231.63	8.31	1229.47	8.17	8.32
62	149	8.31	1237.49	8.30	1236.59	8.17	8.31
62	150	8.30	1245.47	8.29	1243.70	8.17	8.32
62	151	8.29	1251.07	8.28	1250.79	8.17	8.30
62	152	8.28	1259.32	8.28	1257.86	8.17	8.31
63	153	8.27	1265.32	8.27	1264.92	8.16	8.28
62	154	8.27	1273.15	8.26	1271.96	8.17	8.30
63	155	8.26	1279.90	8.25	1278.99	8.16	8.28
64	156	8.26	1288.02	8.24	1286.00	8.14	8.28
64	157	8.24	1294.37	8.24	1293.00	8.14	8.26
64	158	8.24	1302.31	8.23	1299.98	8.14	8.27
65	159	8.23	1308.54	8.22	1306.95	8.12	8.24
66	160	8.23	1316.08	8.21	1313.90	8.11	8.23
65	161	8.21	1322.61	8.20	1320.83	8.12	8.23
66	162	8.21	1330.72	8.20	1327.75	8.11	8.23
66	163	8.20	1336.99	8.19	1334.66	8.11	8.22
66	164	8.20	1344.64	8.18	1341.55	8.11	8.22
67	165	8.19	1350.97	8.17	1348.42	8.09	8.20
68	166	8.18	1358.39	8.16	1355.28	8.07	8.19
68	167	8.17	1364.82	8.16	1362.13	8.07	8.18
68	168	8.17	1372.59	8.15	1368.96	8.07	8.19
68	169	8.16	1378.59	8.14	1375.77	8.07	8.17
68	170	8.15	1385.84	8.13	1382.57	8.07	8.18
69	171	8.14	1392.34	8.12	1389.36	8.06	8.15
70	172	8.14	1399.78	8.12	1396.13	8.04	8.15
70	173	8.13	1406.14	8.11	1402.88	8.04	8.13
70	174	8.12	1413.60	8.10	1409.62	8.04	8.14
70	175	8.11	1419.42	8.09	1416.35	8.04	8.13
70	176	8.10	1426.28	8.09	1423.06	8.04	8.13
71	177	8.09	1432.57	8.08	1429.76	8.03	8.11
72	178	8.09	1440.02	8.07	1436.44	8.01	8.10
72	179	8.08	1446.11	8.06	1443.11	8.01	8.09
72	180	8.07	1453.50	8.05	1449.76	8.01	8.10
73	181	8.06	1459.55	8.05	1456.40	7.99	8.07
74	182	8.06	1466.76	8.04	1463.02	7.98	8.06
74	183	8.05	1472.94	8.03	1469.63	7.98	8.05
74	184	8.05	1480.35	8.02	1476.23	7.98	8.06
74	185	8.03	1486.10	8.02	1482.81	7.98	8.05
74	186	8.03	1493.29	8.01	1489.37	7.98	8.05
75	187	8.02	1499.39	8.00	1495.92	7.96	8.03
76	188	8.01	1506.71	7.99	1502.46	7.94	8.02
76	189	8.00	1512.62	7.98	1508.98	7.94	8.01
76	190	8.00	1520.41	7.98	1515.49	7.94	8.01
76	191	7.99	1526.16	7.97	1521.99	7.94	8.00
76	192	7.99	1533.72	7.96	1528.47	7.94	8.01
77	193	7.98	1539.77	7.95	1534.93	7.93	7.98
78	194	7.98	1547.39	7.95	1541.38	7.91	7.97
78	195	7.97	1553.49	7.94	1547.82	7.91	7.96
78	196	7.97	1561.41	7.93	1554.25	7.91	7.97
79	197	7.96	1567.30	7.92	1560.66	7.90	7.94
78	198	7.95	1574.80	7.91	1567.05	7.91	7.96
79	199	7.95	1581.38	7.91	1573.43	7.90	7.94
80	200	7.95	1589.19	7.90	1579.80	7.88	7.93
80	201	7.94	1595.42	7.89	1586.15	7.88	7.92
80	202	7.94	1603.17	7.88	1592.49	7.88	7.92
80	203	7.93	1609.16	7.88	1598.82	7.88	7.91
80	204	7.92	1616.64	7.87	1605.13	7.88	7.92

Z	A	E_{NEXP1}	E_{BEXP1}	$E_{NTH1new}(A)$	$E_{BTH1new}(A)$	$E_{NTH1new}(Z)$	$E_{NTHLDM}(A,Z)$
81	205	7.92	1623.17	7.86	1611.43	7.87	7.89
82	206	7.92	1630.53	7.85	1617.71	7.85	7.88
82	207	7.91	1637.26	7.85	1623.98	7.85	7.87
83	208	7.91	1644.63	7.84	1630.24	7.83	7.85
82	209	7.89	1648.56	7.83	1636.48	7.85	7.87
82	210	7.87	1653.74	7.82	1642.71	7.85	7.87
83	211	7.86	1658.27	7.81	1648.92	7.83	7.85
84	212	7.85	1664.17	7.81	1655.12	7.82	7.84
84	213	7.83	1668.52	7.80	1661.31	7.82	7.83
84	214	7.82	1674.41	7.79	1667.48	7.82	7.84
85	215	7.81	1678.59	7.78	1673.64	7.80	7.81
86	216	7.80	1684.48	7.78	1679.79	7.79	7.80
86	217	7.78	1689.14	7.77	1685.92	7.79	7.79
86	218	7.78	1695.65	7.76	1692.04	7.79	7.80
86	219	7.76	1700.10	7.75	1698.14	7.79	7.79
86	220	7.76	1706.38	7.75	1704.24	7.79	7.79
87	221	7.74	1711.12	7.74	1710.31	7.77	7.77
88	222	7.74	1717.47	7.73	1716.38	7.75	7.76
88	223	7.72	1722.62	7.72	1722.43	7.75	7.75
88	224	7.72	1729.10	7.72	1728.47	7.75	7.75
88	225	7.71	1734.00	7.71	1734.49	7.75	7.74
88	226	7.70	1740.39	7.70	1740.50	7.75	7.75
89	227	7.69	1745.60	7.69	1746.50	7.74	7.72
90	228	7.68	1752.08	7.69	1752.49	7.72	7.71
90	229	7.67	1757.33	7.68	1758.46	7.72	7.70
90	230	7.67	1764.12	7.67	1764.41	7.72	7.71
90	231	7.66	1769.23	7.66	1770.36	7.72	7.70
90	232	7.65	1775.67	7.66	1776.29	7.72	7.70
91	233	7.64	1781.02	7.65	1782.21	7.71	7.68
92	234	7.64	1787.76	7.64	1788.11	7.69	7.67
92	235	7.63	1793.05	7.63	1794.00	7.69	7.66
92	236	7.63	1799.60	7.63	1799.88	7.69	7.66
92	237	7.61	1804.72	7.62	1805.74	7.69	7.66
92	238	7.61	1810.87	7.61	1811.60	7.69	7.66
94	239	7.60	1816.31	7.60	1817.43	7.66	7.62
94	240	7.60	1822.84	7.60	1823.26	7.66	7.62
94	241	7.59	1828.08	7.59	1829.07	7.66	7.62
94	242	7.58	1834.38	7.58	1834.87	7.66	7.62
94	243	7.57	1839.41	7.57	1840.66	7.66	7.61
96	244	7.56	1845.44	7.57	1846.43	7.63	7.58
96	245	7.55	1850.95	7.56	1852.19	7.63	7.58
96	246	7.55	1857.41	7.55	1857.94	7.63	7.58
96	247	7.54	1862.56	7.55	1863.67	7.63	7.57
96	248	7.54	1868.77	7.54	1869.39	7.63	7.58
97	249	7.52	1873.71	7.53	1875.10	7.62	7.55
98	250	7.52	1879.78	7.52	1880.80	7.60	7.54
98	251	7.51	1884.88	7.52	1886.48	7.60	7.53
98	252	7.50	1891.05	7.51	1892.15	7.60	7.54
98	253	7.49	1895.85	7.50	1897.80	7.60	7.53
98	254	7.49	1901.88	7.49	1903.45	7.60	7.53
99	255	7.48	1906.52	7.49	1909.08	7.58	7.51
100	256	7.47	1912.52	7.48	1914.70	7.57	7.50
100	257	7.46	1917.49	7.47	1920.30	7.57	7.49
100	258	7.46	1923.72	7.46	1925.89	7.57	7.50
100	259	7.45	1928.50	7.46	1931.47	7.57	7.49
100	260	7.44	1934.51	7.45	1937.04	7.57	7.49
101	261	7.43	1939.09	7.44	1942.60	7.55	7.47
102	262	7.42	1944.97	7.44	1948.14	7.54	7.45
102	263	7.41	1950.01	7.43	1953.67	7.54	7.45
102	264	7.41	1956.19	7.42	1959.18	7.54	7.45
103	265	7.40	1960.36	7.41	1964.69	7.52	7.43
104	266	7.39	1965.86	7.41	1970.18	7.51	7.41
104	267	7.38	1970.62	7.40	1975.66	7.51	7.41
104	268	7.38	1976.65	7.39	1981.12	7.51	7.41
105	269	7.36	1980.37	7.39	1986.58	7.49	7.39
106	270	7.35	1985.49	7.38	1992.02	7.48	7.37
106	271	7.34	1990.37	7.37	1997.45	7.48	7.37
106	272	7.34	1996.53	7.36	2002.86	7.48	7.37
106	273	7.33	2001.20	7.36	2008.27	7.48	7.36

Z	A	E_{NEXP1}	E_{BEXP1}	$E_{NTH1new}(A)$	$E_{BTH1new}(A)$	$E_{NTH1new}(Z)$	$E_{NTHLDM}(A,Z)$
107	274	7.32	2004.75	7.35	2013.66	7.46	7.34
107	275	7.31	2010.80	7.34	2019.03	7.46	7.34
108	276	7.30	2015.79	7.33	2024.40	7.45	7.33
107	277	7.30	2021.62	7.33	2029.76	7.46	7.34
108	278	7.29	2026.89	7.32	2035.10	7.45	7.33
108	279	7.28	2031.68	7.31	2040.43	7.45	7.32
108	280	7.28	2037.83	7.31	2045.74	7.45	7.33
109	281	7.26	2041.24	7.30	2051.05	7.43	7.30
109	282	7.26	2046.25	7.29	2056.34	7.43	7.30
110	283	7.25	2051.27	7.28	2061.62	7.42	7.28
110	284	7.25	2057.71	7.28	2066.89	7.42	7.29
111	285	7.23	2060.84	7.27	2072.14	7.40	7.26
111	286	7.22	2066.12	7.26	2077.39	7.40	7.26
112	287	7.21	2070.66	7.26	2082.62	7.39	7.24
112	288	7.21	2077.17	7.25	2087.84	7.39	7.24
113	289	7.20	2079.94	7.24	2093.04	7.37	7.22
113	290	7.19	2085.24	7.24	2098.24	7.37	7.21
114	291	7.18	2089.46	7.23	2103.42	7.36	7.19
115	292	7.16	2091.75	7.22	2108.59	7.34	7.17
116	293	7.15	2095.18	7.21	2113.75	7.33	7.15
117	294	7.13	2096.75	7.21	2118.89	7.31	7.11
118	295	7.12	2099.17	7.20	2124.03	7.30	7.09